

---

# InfoMax-GAN: Improved Adversarial Image Generation via Information Maximization and Contrastive Learning

---

Kwot Sin Lee<sup>1,2</sup> Ngoc-Trung Tran<sup>1</sup> Ngai-Man Cheung<sup>1</sup>

<sup>1</sup>Singapore University of Technology and Design    <sup>2</sup>University of Cambridge  
ks136@cam.ac.uk, {ngoctrung\_tran, ngaiman\_cheung}@sutd.edu.sg

## Abstract

While Generative Adversarial Networks (GANs) are fundamental to many generative modelling applications, they suffer from numerous issues. In this work, we propose a principled framework to simultaneously address two fundamental issues in GANs: catastrophic forgetting of the discriminator and mode collapse of the generator. We achieve this by employing for GANs a contrastive learning and mutual information maximization approach, and perform extensive analyses to understand sources of improvements. Our approach significantly stabilises GAN training and improves GAN performance for image synthesis across *five* datasets under the *same training and evaluation conditions* against state-of-the-art works. Our approach is simple to implement and practical: it involves only one objective, is computationally inexpensive, and is robust across a wide range of hyperparameters *without any tuning*. For reproducibility, our code is available at <https://github.com/kwotsin/mimicry>.

## 1 Introduction

The field of generative modelling has witnessed incredible successes since the advent of Generative Adversarial Networks (GANs) [18], a form of generative model known for its sampling efficiency in generating high-fidelity data [44]. In general, a GAN tries to model the true data distribution of a finite amount of empirical data, and is composed of two models: a generator and a discriminator. The modelling of the distribution is achieved as both models play an adversarial minimax game where the generator tries to fool the discriminator with some fake data generated from sampling a noise prior, and the discriminator tries to avoid being fooled by correctly classifying a given sample as real or fake. This adversarial game is captured by the following equation:

$$\min_G \max_D V(D, G) = \mathbb{E}_{x \sim p_r(x)} [\log D(x)] + \mathbb{E}_{z \sim p(z)} [\log(1 - D(G(z)))] \quad (1)$$

where  $V$  is the value function,  $p(z)$  is a prior noise distribution,  $p_r(x)$  is the real data distribution, and  $G(z)$  represents the generated data after passing some randomly sampled noise  $z$  through the generator  $G$ .

In this minimax formulation, training the discriminator and generator with their respective minimax loss functions aims to minimize the Jensen-Shannon (JS) divergence between the real and generated data distributions [18]  $p_r$  and  $p_g$  respectively. However, GAN training is notoriously difficult. Firstly, such theoretical guarantees only come under the assumption of the discriminator being trained to optimality [21], which may lead to saturating gradients in practice. Even so, there is no guarantee for convergence in this minimax game as both generator and discriminator are simultaneously and independently finding a Nash equilibrium in a high-dimensional space. Finally, GANs face the perennial problem of mode collapse, where  $p_g$  collapses to only cover a few modes of  $p_r$ ,

resulting in generated samples of limited diversity. Consequently, recent years have seen efforts [45, 58, 57, 24, 52, 17, 60] to mitigate these GAN problems, including using gradient matching [58] and a two time-scale update rule [24].

A primary cause of GAN training instability stems from the non-stationary nature of the training environment: as the generator learns, the modeled distribution  $p_g$  the discriminator faces is ever changing. As we represent our GAN models as neural networks, the discriminator neural network is susceptible to *catastrophic forgetting* [39, 11, 29, 26], a situation where the network forgets about prior tasks in order to focus on the current one as the weights of the network updates, which ultimately contributes to training instability. The state-of-the-art Self-supervised GAN (SSGAN) [11] is the first to demonstrate that a representation learning approach could mitigate discriminator catastrophic forgetting, thus improving training stability. However, the approach still does not explicitly mitigate *mode collapse*, and has a failure mode in image generation on datasets involving domains like faces [11]. To address these problems, we present an approach to simultaneously mitigate catastrophic forgetting and mode collapse in GANs, and demonstrate a wide range of practical improvements on natural image synthesis using GANs.

**Our contributions.** (1) We present a GAN framework for improving natural image synthesis through simultaneously mitigating two key GAN issues using just one objective: catastrophic forgetting of the discriminator (via information maximization) and mode collapse of the generator (via contrastive learning). Our approach addresses issues in both discriminator and generator, rather than either alone. (2) With this multi-faceted approach, we demonstrate our framework can significantly improve GAN image synthesis across *five* different datasets against state-of-the-art works under the *same training and evaluation conditions*. (3) Our framework is lightweight and practical: it introduces just one auxiliary objective, has low computational cost, and is robust against a wide range of training hyperparameters *without any tuning* required. (4) Our work is the first to demonstrate the effectiveness of contrastive learning for significantly improving GAN performance, which we hope would open a new research direction in this area.

## 2 Background

**Mutual information and representation learning.** The mutual information between two random variables  $X$  and  $Y$  with marginals  $p(x)$  and  $p(y)$  can be defined as the Kullback-Leibler (KL) divergence between their joint distribution and product of marginals:

$$\begin{aligned} \mathcal{I}(X; Y) &= D_{\text{KL}}(p(x, y) || p(x)p(y)) \\ &= \int_X \int_Y p(x, y) \log \frac{p(x, y)}{p(x)p(y)} dy dx \end{aligned} \quad (2)$$

Intuitively, for some random variable  $Y$  that is independent of  $X$ , we have  $p(x, y) = p(x)p(y)$ , rendering the log term to be 0 and thus  $\mathcal{I}(X; Y) = 0$ . Viewed from this perspective, mutual information is non-negative and represents the amount of information one gains about a random variable from the knowledge of another random variable.

While mutual information is a straightforward concept, it has been strongly tied to representation learning [5], where we aim to learn an encoder function  $E$  that ideally captures the most important features of the input data  $X$ , often at a lower dimensional latent space. This concept is encapsulated by the InfoMax objective [34]:

$$\max_{E \in \mathcal{E}} \mathcal{I}(X; E(X)) \quad (3)$$

where  $\mathcal{E}$  is some function class, and the objective is to find some  $E$  that maximizes the mutual information between the input data and its encoded representations  $E(X)$ . To maximize on the InfoMax objective, one could alternatively maximize  $\mathcal{I}(C_\psi(X); E_\psi(X))$ , where  $C_\psi$  and  $E_\psi$  are encoders part of the same architecture parameterised by  $\psi$ . It can be shown in [61] maximizing  $\mathcal{I}(C_\psi(X); E_\psi(X))$  is maximizing on a lower bound of the InfoMax objective:

$$\mathcal{I}(C_\psi(X); E_\psi(X)) \leq \mathcal{I}(X; (C_\psi(X), E_\psi(X))) \quad (4)$$

In practice, as noted in [61, 49], maximizing  $\mathcal{I}(C_\psi(X); E_\psi(X))$  has several advantages: (a) Using different feature encodings allow us to capture different views and modalities of the data for flexibility of modelling [3, 55]; (b) The encoded data lies in a much lower dimensional latent space than that of the original data, thus reducing computational constraints.

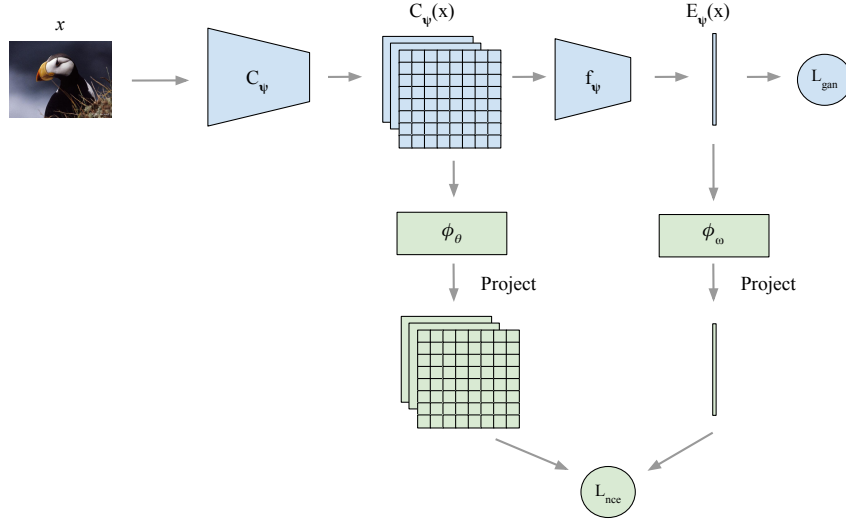


Figure 1: Illustration of the InfoMax-GAN framework. A real or fake image  $x$  passes through a discriminator encoder  $E_\psi = f_\psi \circ C_\psi$ , producing local feature map  $C_\psi(x)$  and global feature vector  $E_\psi(x)$ , which are then each projected to a higher dimension by critic networks  $\phi_\theta$  and  $\phi_\omega$  to compute the InfoNCE loss for the InfoMax objective. The framework merely produces a constraint on the features produced by the discriminator, and requires no modification to the GAN architecture.

**Contrastive learning.** An emerging theme in recent state-of-the-art works in unsupervised representation learning [3, 46, 25, 23, 55, 36, 30] lies in taking a contrastive approach to maximizing the mutual information between encoded local and global features. Yet, since directly maximizing mutual information is often intractable in practice [47], these works often maximize on the InfoNCE [46] lower bound instead, which involves a contrastive loss minimized through having a critic correctly finding a positive sample in contrast to a set of negative samples. Such positive/negative samples can be arbitrarily created by pairing features [25], augmentation [10], or a combination of both [3]. Our work similarly maximizes on this InfoNCE bound, and most closely follows the Deep InfoMax [25] approach of obtaining local and global features for the maximization, for which the reader is highly encouraged to read.

### 3 InfoMax-GAN

In this section, we first explain our approach and its benefits in alleviating two key issues of GANs.

#### 3.1 Approach

Figure 1 illustrates the InfoMax-GAN framework. Firstly, to maximize on the lower bound of the InfoMax objective,  $\mathcal{I}(C_\psi(X); E_\psi(X))$ , we set  $E_\psi$  to represent layers of a GAN discriminator leading to the global features, and  $C_\psi$  as layers leading to the local features.

To estimate  $\mathcal{I}(C_\psi(X); E_\psi(X))$  in practice, we use the InfoNCE loss, which was theoretically shown to maximize on a lower bound of this mutual information [46]. Formally, for some set of  $N$  random images  $X = \{x_1, \dots, x_N\}$  and set  $\mathcal{A} = \{0, 1, \dots, M^2 - 1\}$  representing indices of a  $M \times M$  spatial sized local feature map, we define the InfoNCE loss in this paper as:

$$\begin{aligned} L_{nce}(X) &= -\mathbb{E}_{x \in X} \mathbb{E}_{i \in \mathcal{A}} \left[ \log p(C_\psi^{(i)}(x), E_\psi(x) | X) \right] \\ &= -\mathbb{E}_{x \in X} \mathbb{E}_{i \in \mathcal{A}} \left[ \log \frac{\exp(g_{\theta, \omega}(C_\psi^{(i)}(x), E_\psi(x)))}{\sum_{(x', i) \in X \times \mathcal{A}} \exp(g_{\theta, \omega}(C_\psi^{(i)}(x'), E_\psi(x)))} \right] \end{aligned} \quad (5)$$

where  $g_{\theta, \omega} : \mathbb{R}^{1 \times 1 \times K} \times \mathbb{R}^{1 \times 1 \times K} \rightarrow \mathbb{R}$  is a critic mapping the local and global features to a scalar score, for some local and global feature vectors with  $K$  dimensions. Formally, we can define  $g_{\theta, \omega}$  to

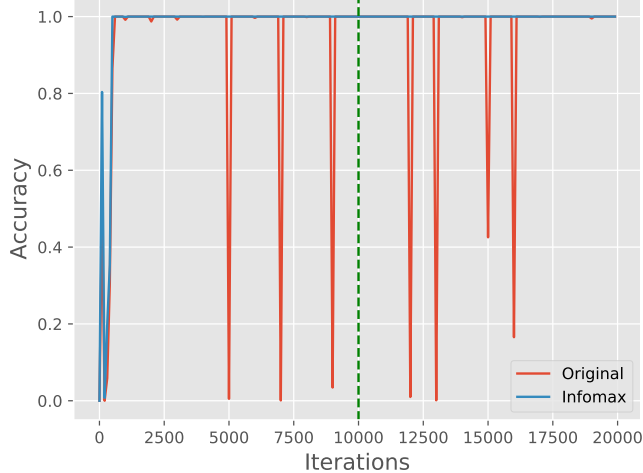


Figure 2: Accuracy of a classifier when trained on the one-vs-all CIFAR-10 classification task. Regularized with the InfoMax objective by minimizing (5), the classifier successfully predicts classes trained from previous iterations even when the underlying class distribution changes.

be:

$$g_{\theta,\omega}(C_{\psi}^{(i)}(x), E_{\psi}(x)) = \phi_{\theta}(C_{\psi}^{(i)}(x))^T \phi_{\omega}(E_{\psi}(x)) \quad (6)$$

where  $\phi_{\theta} : \mathbb{R}^{M \times M \times K} \rightarrow \mathbb{R}^{M \times M \times R}$  and  $\phi_{\omega} : \mathbb{R}^{1 \times 1 \times K} \rightarrow \mathbb{R}^{1 \times 1 \times R}$  are separate functions parameterized by  $\theta$  and  $\omega$  respectively, projecting the local and global features to a higher Reproducing Kernel Hilbert Space (RKHS) [2] dimension  $R$  to exploit the value of the linear evaluation. In practice,  $\phi_{\theta}$  and  $\phi_{\omega}$  are defined as shallow networks with only 1 hidden layer following [25], but with spectral normalized weights as well.

Intuitively,  $\forall x, x' \in X$ , and  $\forall i, j \in \mathcal{A}, i \neq j$ , the InfoNCE task requires the critic  $g_{\theta,\omega}$  to distinguish the positive sample pair  $(C_{\psi}^{(i)}(x), E_{\psi}(x))$  sampled from the joint distribution apart from the negative sample pairs  $(C_{\psi}^{(j)}(x'), E_{\psi}(x))$  sampled from the product of marginals, in order to maximize mutual information between the local and global features.

To stabilize training, we constrain the discriminator to learn from only the InfoNCE loss of real image features, and similarly for the generator, from only the InfoNCE loss of fake image features. We formulate the losses for discriminator and generator  $L_D$  and  $L_G$  as such:

$$L_G = L_{\text{gan}}(\hat{D}, G) + \alpha L_{\text{ncc}}(X_g) \quad (7)$$

$$L_D = L_{\text{gan}}(D, \hat{G}) + \beta L_{\text{ncc}}(X_r) \quad (8)$$

where  $\alpha$  and  $\beta$  are hyperparameters;  $L_{\text{gan}}$  is the hinge loss for GANs as used in [41];  $\hat{D}$  and  $\hat{G}$  represent a fixed discriminator and generator respectively;  $X_r$  and  $X_g$  represent sets of real and generated images respectively. In practice, we set  $\alpha = \beta = 0.2$  for all experiments for simplicity, with ablation studies to show our approach is robust across a wide range of  $\alpha$  and  $\beta$  values.

Intuitively, our approach improves discriminator representation learning as the global feature representations – which are also used for solving the GAN objective – are constrained to have high mutual information with all local features of the same image, which essentially produces descriptive global features representing the whole image for solving the GAN task, leading to more informative gradient feedback. Furthermore, to prevent the network from cheating, the feature vectors sampled from the same local feature map are also treated as negative samples for any local feature vector. Doing so, the global features are constrained to have consistently high mutual information with *all* local features from the same image, rather than only specific ones (e.g. those representing background) that are trivial to solve.

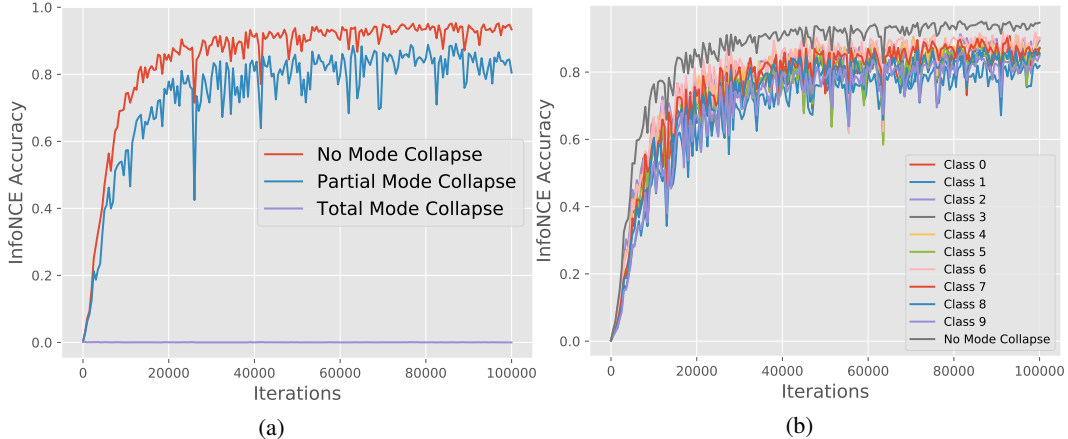


Figure 3: InfoNCE task accuracy when simulating generators exhibiting a range of mode collapse behaviours. (a) We show that the less mode collapsed a generator is, the better the accuracy for InfoNCE. (b) The InfoNCE accuracy is consistently lower when the generator has partially mode collapsed to any individual class, compared to when there is no mode collapse.

### 3.2 Mitigating Catastrophic Forgetting

Our approach mitigates a key issue in GANs: *catastrophic forgetting* of the discriminator, a situation where due to the non-stationary nature of the training environment, the discriminator learns only ad-hoc representations and forget about prior tasks it was trained on. For instance, while the discriminator may learn to penalize flaws in global structures early in GAN training [11], it may later forget these relevant representations in order to learn those for finding detailed flaws in local structures, which overall contributes to training instability.

Similar to [11], we examine the ability of our approach in mitigating catastrophic forgetting: we train a discriminator classifier on the one-vs-all CIFAR-10 classification task where the underlying class distribution changes every 1K iterations, and the cycle repeats every 10K iterations. As seen in Figure 2, without the InfoMax objective, the classifier can overfit to a certain class distribution and produce very low accuracy when the class distribution is changed. When training is regularized with the InfoMax objective, the classifier successfully remembers all prior classes it was trained on. Thus, the InfoMax objective helps the discriminator to reduce catastrophic forgetting and adapt to the non-stationary nature of the generated image distribution, which ultimately stabilizes GAN training.

### 3.3 Mitigating Mode Collapse

Our approach also mitigates a persistent problem of the generator: *mode collapse*. For a fully mode collapsed generator, we have  $x = x' \forall x, x' \sim X_g$ , where  $X_g$  is a set of randomly generated images, such that  $C_\psi(x) = C_\psi(x')$ . This means the term  $p(C_\psi^{(i)}(x), E_\psi(x) | X_g)$  approaches 0 in the limit, rather than the optimal value 1, as the critics are not able to distinguish apart the multiple identical feature pairs from individual images.

To validate this, we show there is a direct correlation between the diversity of generated images and the contrastive learning task accuracy  $p(C_\psi^{(i)}(x), E_\psi(x) | X)$ . We train the discriminator to solve the InfoNCE task using CIFAR-10 training data, and simulate 3 different kinds of generators using CIFAR-10 test data: (a) a perfect generator with no mode collapse that can generate *all classes of images*; (b) a partially mode collapsed generator that can only generate *one class of images* and (c) a totally mode collapsed generator that can only generate *one image*.

From Figure 3a, we observe a perfect generator with no mode collapse best solves the InfoNCE task, and a partially mode collapsed generator has a consistently poorer accuracy in the InfoNCE task than the perfect generator. This concurs with our expectation: images from only one class exhibit a much lower diversity than images from all classes, and so distinguishing the positive samples amongst similar and harder negative samples results in greater difficulty in solving the InfoNCE task.

Furthermore, for a totally mode collapsed generator which can only generate one image, we observe the accuracy is *near zero*, which confirms our initial hypothesis. For any  $N$  images, there are  $NM^2$  samples to classify in the InfoNCE task, with  $NM^2 - 1$  negative samples for each positive sample. However, if all  $N$  images are identical due to total mode collapse, then there exists  $N - 1$  negative samples identical to each positive sample, which makes the InfoNCE task nearly impossible to solve. Thus, to solve the InfoNCE task well, the generator is highly encouraged to generate images with greater diversity, which reduces mode collapse.

Furthermore, from Figure 3b, we see the performance of any individual class demonstrating partial mode collapse is *consistently worse* than the case of no mode collapse, where all classes of images are used. Thus, the generator is incentivised to not collapse to producing just any one class that can fool the discriminator easily, since producing *all classes* of images would naturally lead to the best performance in the contrastive task.

## 4 Experiments

### 4.1 GAN Architectures

To evaluate our approach, we experiment with Spectral Normalization GAN (SNGAN) [41] and the state-of-the-art Self-supervised GAN (SSGAN) [11]. SNGAN is an unconditional GAN utilizing spectral normalization to stabilize GAN training by constraining the discriminator to be 1-Lipschitz, and has been the basis of recent state-of-the-art GANs [42, 63, 8, 16]. SSGAN is the state-of-the-art unconditional GAN that has achieved a highly competitive performance compared to conditional GANs of the same architectural capacity. SSGAN does not utilise human-annotated labels, but performs 4 different rotations on the images to obtain pseudo-labels for classifying the images’ rotations to improve GAN performance. We emphasize all three GANs experimented are *unconditional*, meaning they do not require conditioning on labeled data.

For clarity, we highlight here that InfoMax-GAN is equivalent to SNGAN with the InfoNCE task objective, and SSGAN is equivalent to SNGAN with the rotation task objective. We show that InfoMax-GAN *alone* is able to achieve highly competitive performance and significant improvements over SSGAN. We detail the exact architectures used for all models and datasets in Appendix C.

### 4.2 Experimental Settings

**Datasets.** We evaluate our models across five different datasets: ImageNet [14], CelebA [35], CIFAR-10 [31], STL-10 [13], and CIFAR-100 [31]. For preprocessing our images, we follow settings in [42, 11]. For ImageNet, we use the 1.3M training images downsampled to size  $128 \times 128$ . For CelebA, we use the aligned version of the 200K images downsampled to size  $128 \times 128$ . For CIFAR-10 and CIFAR-100 we use all 50K training images, and for STL-10, we use all 100K unlabeled images downsampled to size  $48 \times 48$ .

**Training.** For all models, we use Residual Network [22] backbones following [41]. For all datasets, we adopt the Adam optimizer [28] with a learning rate of  $2 \times 10^{-4}$  and batch size of 64, following [21, 41]. For CIFAR-10, CIFAR-100 and STL-10, we follow settings in [42] by linearly decaying learning rate over 100K generator steps, each taken every 5 discriminator update steps. For ImageNet, we follow [41] by increasing the number of generator updates to 450K steps instead, but with no learning rate decay. For CelebA, we follow [11] by taking 100K generator steps, each taken after 2 discriminator updates and with no learning rate decay.

For all models and datasets, we set  $\alpha = \beta = 0.2$ , to balance the InfoNCE loss to be on the same scale as the GAN loss initially. This scaling principle is similar to what is applied in [12], with details in Appendix A.1. We further perform ablation studies for  $\alpha$  and  $\beta$  to show our framework is robust to changes in these hyperparameters. Finally, for fairness in our comparisons, we re-implemented all considered models using the same code base and framework, and conducted all experiments under the *same training conditions*.

**Evaluation.** To assess the quality of generated images against the real images, we compute the Fréchet Inception Distance (FID). Formally, the FID computes the Wasserstein-2 Distance between

Metric	Dataset	Resolution	Models		
			SNGAN	SSGAN	InfoMax-GAN
FID	ImageNet	128 × 128	65.74 ± 0.31	62.48 ± 0.31	<b>58.91 ± 0.14</b>
	CelebA	128 × 128	14.04 ± 0.02	16.39 ± 0.09	<b>10.63 ± 0.04</b>
	STL-10	48 × 48	40.48 ± 0.07	38.97 ± 0.23	<b>37.49 ± 0.05</b>
	CIFAR-100	32 × 32	24.76 ± 0.16	24.64 ± 0.16	<b>21.22 ± 0.26</b>
	CIFAR-10	32 × 32	18.63 ± 0.22	<b>16.59 ± 0.13</b>	17.14 ± 0.20

Table 1: Mean FID scores (lower is better) of all models across different datasets, computed across 3 different seeds.

features produced by a pre-trained Inception [54] network for input real and generated images:

$$d_{\text{FID}} = \|\mu_r - \mu_g\|_2^2 + \text{Tr}(\Sigma_r + \Sigma_g - 2(\Sigma_r \Sigma_g)^{\frac{1}{2}}) \quad (9)$$

where  $\mu_r$  and  $\Sigma_r$  denotes the mean and covariance of feature vectors produced by forwarding real images through a pre-trained Inception [54] network, and  $\mu_g$  and  $\Sigma_g$  similarly represents the equivalent for fake images. For all FID scores reported in this paper, we compute them using 50K real samples and 10K fake samples across 3 random seeds to report the mean and standard deviation of the scores. As 50K real samples are much lesser than the 1.3M images in ImageNet, we randomly sample without replacement 50 images from each of the 1000 classes to compute the real image statistics, to avoid high bias in the results. We emphasize that for fairness in comparisons, we used the same number of real and fake samples when computing FID, since FID can produce highly bias estimates at different sample sizes [7].

### 4.3 Results

**Improved image synthesis.** As seen in Table 1, InfoMax-GAN achieves a consistent and significant improvement in FID across all datasets over the baseline SNGAN, and significantly so over SSGAN on multiple datasets. On the challenging high resolution ImageNet dataset, InfoMax-GAN improves by **6.8 points** over SNGAN, and **3.6 points** over SSGAN. On the high resolution CelebA, while SSGAN could not improve over the baseline SNGAN, as similarly noted in [11], InfoMax-GAN improves by **3.4 points** over SNGAN, and **5.8 points** over SSGAN. This suggests our approach is versatile and can generalise across multiple data domains.

On STL-10, InfoMax-GAN achieves an improvement of **3.0 points** over SNGAN and **1.5 points** over SSGAN. Interestingly, while InfoMax-GAN performs similarly as SSGAN on CIFAR-10 with around **0.5 points** difference, it is able to achieve **3.4 points** improvements on CIFAR-100 when the number of classes increase. We conjecture this is due to the tendency for SSGAN to generate images that are easy to rotate [59], which sacrifices diversity and reduces FID when there are more classes. This observation also supports InfoMax-GAN’s larger improvements on ImageNet, which has 1000 classes. We provide image samples randomly generated by InfoMax-GAN for all datasets in Appendix A.2.

Finally, we show that our improvements are orthogonal to that in SSGAN in Table 2: when incorporating our objective into SSGAN, FID is improved across all datasets significantly, achieving even larger improvements for the challenging ImageNet dataset. Thus, our method is flexible and can be easily integrated into existing state-of-the-art frameworks like SSGAN.

**Improved training stability.** Similar to [11], we test training stability through evaluating the sensitivity of model performance when hyperparameters are varied across a range of popular settings for training GANs, such as the Adam parameters  $(\beta_1, \beta_2)$  and number of discriminator steps per generator step,  $n_{\text{dis}}$ . These sets of hyperparameters are based on settings in [11, 41, 21, 62, 50], which are well-tested settings used in popular works such as SNGAN and WGAN-GP [21]. As seen in Table 3, in comparison to SNGAN at the *same architectural capacity*, InfoMax-GAN obtains a consistent FID improvement for different datasets even in instances where GAN training does not converge (e.g. when  $n_{\text{dis}} = 1$ ). The variability in FID scores for the InfoMax-GAN variants is much lower than SNGAN, showing its robustness to changes in training hyperparameters. Finally, we observe

Dataset	Resolution	Models	
		SSGAN	SSGAN + IM
ImageNet	128 × 128	62.48 ± 0.31	<b>56.45 ± 0.29</b>
CelebA	128 × 128	16.39 ± 0.09	<b>11.93 ± 0.14</b>
STL-10	48 × 48	38.97 ± 0.23	<b>37.73 ± 0.06</b>
CIFAR-100	32 × 32	24.64 ± 0.16	<b>21.40 ± 0.20</b>
CIFAR-10	32 × 32	16.59 ± 0.13	<b>15.42 ± 0.08</b>

Table 2: Mean FID scores (lower is better) of SSGAN before and after applying our method: “+ IM” refers to adding our proposed InfoMax-GAN objective. Our improvement is orthogonal to that of SSGAN and can be easily integrated into existing frameworks.

$\beta_1$	$\beta_2$	$n_{\text{dis}}$	CIFAR-10		STL-10	
			SNGAN	InfoMax-GAN	SNGAN	InfoMax-GAN
0.0	0.9	1	164.74 ± 0.42	<b>24.42 ± 0.18</b>	267.10 ± 0.20	<b>54.29 ± 0.13</b>
0.0	0.9	2	20.87 ± 0.19	<b>18.08 ± 0.27</b>	46.65 ± 0.18	<b>38.96 ± 0.31</b>
0.0	0.9	5	18.63 ± 0.22	<b>17.14 ± 0.20</b>	40.48 ± 0.07	<b>37.49 ± 0.05</b>
0.5	0.999	1	73.07 ± 0.20	<b>20.58 ± 0.10</b>	134.51 ± 0.37	<b>62.28 ± 0.07</b>
0.5	0.999	2	18.74 ± 0.24	<b>17.19 ± 0.32</b>	40.67 ± 0.29	<b>40.54 ± 0.20</b>
0.5	0.999	5	21.10 ± 0.89	<b>18.39 ± 0.04</b>	84.20 ± 0.67	<b>75.72 ± 0.19</b>

Table 3: Mean FID scores (lower is better) across a range of hyperparameter settings.  $(\beta_1, \beta_2)$  represents the hyperparameters of the Adam optimizer, and  $n_{\text{dis}}$  represents the number of discriminator steps per generator step. Our method performs robustly in a wide range of training settings *without any tuning*.

while different sets of  $(\beta_1, \beta_2)$  work better for each dataset, our method is able to stabilize training and obtain significant improvements in all these settings, *without any hyperparameter tuning*.

In Figure 4, we show that our method greatly stabilises GAN training to achieve a faster convergence of GAN training early on, with a consistent improvement throughout the training process. We attribute this to the fact that under an additional constraint where the global features of images are

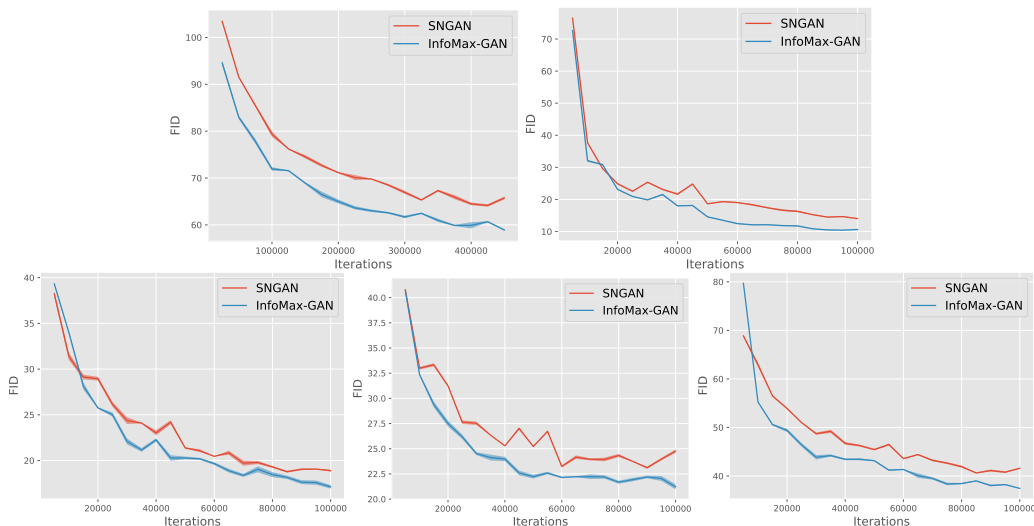


Figure 4: Our approach stabilises GAN training significantly to achieve a faster convergence and consistent improvement in FID for all models across all datasets. Top row: ImageNet, CelebA. Bottom row: CIFAR-10, CIFAR-100, STL-10.

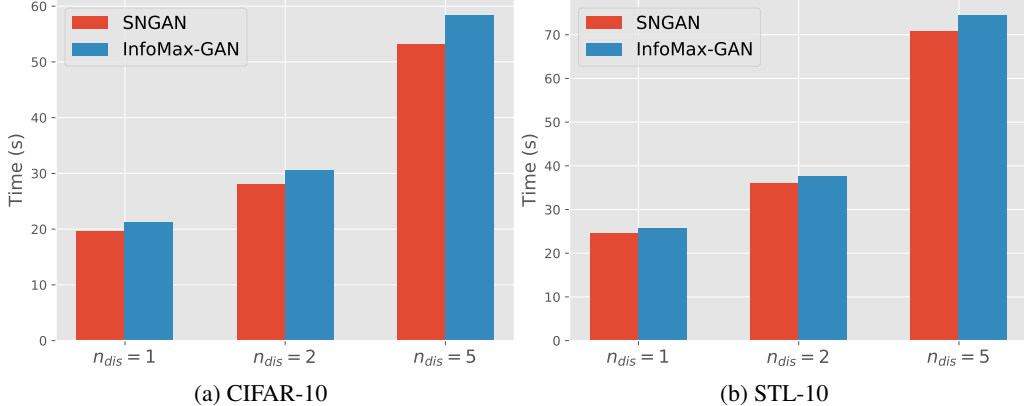


Figure 5: Training time for 100 generator update steps across different  $n_{dis}$  values for CIFAR-10 and STL-10, as computed using the same hardware. In general, our proposed framework incurs significantly less time than the overall training cost.

Metric	K	DCGAN	DCGAN + IM
# Modes	1/4	27.67 ± 0.47	<b>62.00 ± 1.63</b>
# Modes	1/2	610.00 ± 8.83	<b>716.67 ± 1.25</b>
$\mathcal{D}_{KL}(p  q)$	1/4	5.44 ± 0.01	<b>4.68 ± 0.01</b>
$\mathcal{D}_{KL}(p  q)$	1/2	1.98 ± 0.01	<b>1.64 ± 0.01</b>

Table 4: Number of modes (higher is better) recovered by the generator on the Stacked MNIST dataset, where the maximum value is 1000; and KL divergence  $\mathcal{D}_{KL}(p||q)$  between the distribution of generated modes  $p$  and the uniform distribution  $q$ , where lower is better. ‘+ IM’ refers to adding our proposed InfoMax-GAN objective.

constrained to have high mutual information with all their local features [25], the space of generated data distribution  $p_g$  is also constrained, thereby causing  $p_g$  to change less radically and ultimately stabilising the GAN training environment.

**Low computational cost.** In practice, our method takes only a fraction of the training time. Similar to [41], we show this by profiling the training time for 100 generator update steps. From Figure 5, we see our approach takes up minimal time at less than 0.1% of training time per update, across all  $n_{dis}$  for both CIFAR-10 and STL-10. This is because in practice, we only need 2 shallow (1 hidden layer) MLP networks to compute the InfoNCE loss. Furthermore, from Table 3, we note that at  $n_{dis} = 2$ , InfoMax-GAN has a consistently better FID than SNGAN at  $n_{dis} = 5$  at approximately *half the training time*, since a large  $n_{dis}$  is a significant bottleneck in training time. Thus, our approach is practical for training GANs with less time taken, and with minimal computational overhead, our method can be easily integrated into existing frameworks without becoming a bottleneck.

**Improved mode recovery.** Following settings in [40], we re-implement the DCGAN [50] in [40] and evaluate its ability in recovering all 1000 modes of the Stacked MNIST dataset [40], composed by randomly stacking 3 grayscale MNIST [33] digits into an RGB image, resulting in 1000 possible modes. We use a pre-trained MNIST classifier to classify each color channel of a generated image, and the model is said to recover 1 mode if it generates at least 1 image for that mode. We similarly set  $K \in \{\frac{1}{4}, \frac{1}{2}\}$ , where  $K$  indicates the size of the discriminator relative to the generator. Intuitively, the smaller  $K$  is, the easier it is for the generator to fool the discriminator with just a few modes, resulting in less modes recovered. Furthermore, we compute the KL divergence  $\mathcal{D}_{KL}(p||q)$  between the generated mode distribution  $p$  and optimal uniform distribution of the modes  $q$ . We see from Table 4 that our method helps to recover more modes for all  $K$ , with the recovered distribution having a consistently lower KL divergence with the ideal uniform distribution as a result.

$R$	Relative Size	FID Score
256	2	$17.07 \pm 0.25$
512	4	$17.21 \pm 0.15$
1024	8	$17.14 \pm 0.20$
2048	16	$17.80 \pm 0.05$
4096	32	$17.38 \pm 0.11$

Table 5: Mean FID scores (lower is better) for InfoMax-GAN on CIFAR-10 when the RKHS dimension  $R$  is varied. Relative size here refers to how much larger  $R$  is relative to the discriminator feature map depth of 128, in terms of multiplicative factor.

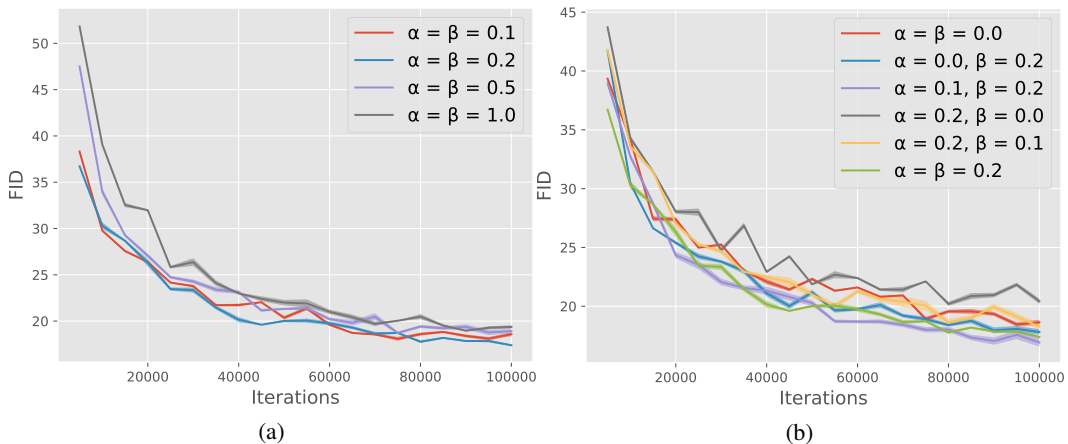


Figure 6: (a) CIFAR-10 FID curves for InfoMax-GAN across a large sweep of  $\alpha$  and  $\beta$  hyperparameters, showing  $\alpha = \beta = 0.2$  performs the best. However, the overall performance remains approximately similar. (b) We perform a small sweep around the chosen hyperparameters  $\alpha = \beta = 0.2$ .

#### 4.4 Ablation Studies

**RKHS dimensions.** As seen in Table 5, our proposed framework is robust to the choice of  $R$ , with the FID remaining consistent in their range of values. We attribute this to the fact that the InfoMax critics are simple MLP networks with only 1 hidden layer, which is sufficient for achieving good representations in practice [61]. We note for all our experiments in Tables 1 and 3, we used  $R = 1024$ .

**Sensitivity of  $\alpha$  and  $\beta$  hyperparameters.** In Figure 6a, we performed a large sweep of  $\alpha$  and  $\beta$  from 0.0 to 1.0, and see that  $\alpha = \beta = 0.2$  obtains the best performance for our method. From Figure 6b, we observe our InfoMax objective for the discriminator is important for improving GAN performance: as  $\beta$  is decreased, keeping  $\alpha = 0.2$ , FID deteriorates. Interestingly, we observe when  $\alpha = 0$  and  $\beta = 0.2$ , having the InfoMax objective for the discriminator alone is sufficient in gaining FID improvements. This confirms our intuition of the role of information maximization in mitigating discriminator catastrophic forgetting to stabilize the GAN training environment to improve FID. However, the performance improves when the generator is also trained on the InfoMax objective, at  $\alpha \in \{0.1, 0.2\}$  and  $\beta = 0.2$ , which affirms our prior intuition that the contrastive nature of the objective helps the generator reduce mode collapse and improve FID. We note that apart from this ablation study, we used  $\alpha = \beta = 0.2$  for all experiments reported in this paper.

## 5 Related Work

**Mode collapse and catastrophic forgetting.** Early works in reducing mode collapse include Unrolled GAN [40], which restructures the generator objective with respect to unrolled discriminator optimization updates. These works often focused on assessing the number of modes recovered by a GAN based on synthetic datasets [53, 40, 9]. Subsequent works include MSGAN [37], which

introduces a regularization encouraging conditional GANs to seek out minor modes often missed when training. These works instead focus on direct metrics [24, 7, 51, 52, 32, 20] for assessing the diversity and quality of generated images. In our work, we utilized both types of metrics for assessment. Previous approaches to mitigate catastrophic forgetting in GANs include using forms of memory [19, 27, 52], such as checkpoint averaging. [11] demonstrates the mitigation of catastrophic forgetting using a representation learning approach, which we built upon.

**Representation learning and GANs.** To the best of our knowledge, the closest work in *methodology* to ours is the state-of-the-art Self-Supervised GAN (SSGAN), which demonstrates the use of a representation learning approach of predicting rotations [15] to mitigate GAN forgetting and hence improve GAN performance. In contrast to SSGAN, our work uses a contrastive learning and information maximization task instead, which we demonstrate to simultaneously mitigate *both* GAN forgetting and mode collapse. Furthermore, our work is able to overcome failure modes demonstrated in SSGAN, such as in datasets involving faces [11]. For fair comparisons, our work compared with SSGAN using the *exact* same architectural capacity, training and evaluation settings.

**Information theory and GANs.** The most prominent work in utilising mutual information maximization for GANs is InfoGAN, but we emphasize here that our work has a *different focus*: while InfoGAN focuses on learning disentangled representations, our goal is to improve image synthesis. For clarity, we illustrate the specific differences with InfoGAN in Appendix B. Other approaches employing information theoretic principles include Variational GAN (VGAN) [48], which uses an information bottleneck [56] to regularize the discriminator representations; with [6, 38, 43] extending to minimise divergences apart from the original JS divergence. In contrast to these works, our work employs the InfoMax principle to improve discriminator learning, and provides a clear connection to how this improves GAN training via the mitigation of catastrophic forgetting.

## 6 Conclusion and Future Work

In this paper, we presented the InfoMax-GAN framework for improving natural image synthesis through simultaneously alleviating two key issues in GANs: catastrophic forgetting of the discriminator (via information maximization), and mode collapse of the generator (via contrastive learning). Our approach significantly improves on the natural image synthesis task for *five* widely used datasets, and further overcome failure modes in state-of-the-art models like SSGAN. Our approach is practical: it performs robustly in a wide range of training settings without any hyperparameter tuning, has low computational cost, and demonstrated improvements even when integrated to existing state-of-the-art models like SSGAN. As future work, it would be interesting to explore this framework for different tasks, such as in 3D view synthesis, where one could formulate objectives involving mutual information and adjacent views.

To the best of our knowledge, our work is the first to investigate using information maximization and contrastive learning to improve GAN image synthesis performance, and we hope our work opens up new possibilities in this direction.

## Acknowledgements

The authors thank Ting Chen for the helpful discussions and information on running the catastrophic forgetting experiment.

## References

- [1] GANs with Spectral Normalization and Projection Discriminator. [https://github.com/pfnet-research/sngan\\_projection](https://github.com/pfnet-research/sngan_projection). Accessed: 2019-10-31.
- [2] Nachman Aronszajn. Theory of Reproducing Kernels. *Transactions of the American Mathematical Society*, 68(3):337–404, 1950.
- [3] Philip Bachman, R Devon Hjelm, and William Buchwalter. Learning Representations by Maximizing Mutual Information Across Views. *arXiv Preprint arXiv:1906.00910*, 2019.

- [4] David Barber and Felix V Agakov. The IM Algorithm: A Variational Approach to Information Maximization. In *Advances in Neural Information Processing Systems*, page None, 2003.
- [5] Yoshua Bengio, Aaron Courville, and Pascal Vincent. Representation Learning: A Review and New Perspectives. *IEEE Transactions on Pattern Analysis and Machine Intelligence*, 35(8):1798–1828, 2013.
- [6] Himesh Bhatia, William Paul, Fady Alajaji, Bahman Ghahserifard, and Philippe Burlina. R\{e}nyi Generative Adversarial Networks. *arXiv preprint arXiv:2006.02479*, 2020.
- [7] Mikołaj Bińkowski, Dougal J Sutherland, Michael Arbel, and Arthur Gretton. Demystifying Mmd Gans. *arXiv Preprint arXiv:1801.01401*, 2018.
- [8] Andrew Brock, Jeff Donahue, and Karen Simonyan. Large Scale Gan Training for High Fidelity Natural Image Synthesis. *arXiv Preprint arXiv:1809.11096*, 2018.
- [9] Tong Che, Yanran Li, Athul Paul Jacob, Yoshua Bengio, and Wenjie Li. Mode Regularized Generative Adversarial Networks. *arXiv Preprint arXiv:1612.02136*, 2016.
- [10] Ting Chen, Simon Kornblith, Mohammad Norouzi, and Geoffrey Hinton. A Simple Framework for Contrastive Learning of Visual Representations. *arXiv Preprint arXiv:2002.05709*, 2020.
- [11] Ting Chen, Xiaohua Zhai, Marvin Ritter, Mario Lucic, and Neil Houlsby. Self-Supervised Gans via Auxiliary Rotation Loss. In *Proceedings of the IEEE Conference on Computer Vision and Pattern Recognition*, pages 12154–12163, 2019.
- [12] Xi Chen, Yan Duan, Rein Houthoofd, John Schulman, Ilya Sutskever, and Pieter Abbeel. Infogan: Interpretable Representation Learning by Information Maximizing Generative Adversarial Nets. In *Advances in Neural Information Processing Systems*, pages 2172–2180, 2016.
- [13] Adam Coates, Andrew Ng, and Honglak Lee. An Analysis of Single-Layer Networks in Unsupervised Feature Learning. In *Proceedings of the Fourteenth International Conference on Artificial Intelligence and Statistics*, pages 215–223, 2011.
- [14] Jia Deng, Wei Dong, Richard Socher, Li-Jia Li, Kai Li, and Li Fei-Fei. Imagenet: A Large-Scale Hierarchical Image Database. In *2009 IEEE Conference on Computer Vision and Pattern Recognition*, pages 248–255. Ieee, 2009.
- [15] Spyros Gidaris, Praveer Singh, and Nikos Komodakis. Unsupervised Representation Learning by Predicting Image Rotations. *arXiv Preprint arXiv:1803.07728*, 2018.
- [16] Xinyu Gong, Shiyu Chang, Yifan Jiang, and Zhangyang Wang. AutoGAN: Neural Architecture Search for Generative Adversarial Networks. *arXiv Preprint arXiv:1908.03835*, 2019.
- [17] Ian Goodfellow. NIPS 2016 Tutorial: Generative Adversarial Networks. *arXiv Preprint arXiv:1701.00160*, 2016.
- [18] Ian Goodfellow, Jean Pouget-Abadie, Mehdi Mirza, Bing Xu, David Warde-Farley, Sherjil Ozair, Aaron Courville, and Yoshua Bengio. Generative Adversarial Nets. In *Advances in Neural Information Processing Systems*, pages 2672–2680, 2014.
- [19] Paulina Grnarova, Kfir Y Levy, Aurelien Lucchi, Thomas Hofmann, and Andreas Krause. An Online Learning Approach to Generative Adversarial Networks. *arXiv Preprint arXiv:1706.03269*, 2017.
- [20] Paulina Grnarova, Kfir Y Levy, Aurelien Lucchi, Nathanael Perraudin, Ian Goodfellow, Thomas Hofmann, and Andreas Krause. A Domain Agnostic Measure for Monitoring and Evaluating GANs. In *Advances in Neural Information Processing Systems*, pages 12069–12079, 2019.
- [21] Ishaan Gulrajani, Faruk Ahmed, Martin Arjovsky, Vincent Dumoulin, and Aaron C Courville. Improved Training of Wasserstein Gans. In *Advances in Neural Information Processing Systems*, pages 5767–5777, 2017.
- [22] Kaiming He, Xiangyu Zhang, Shaoqing Ren, and Jian Sun. Deep Residual Learning for Image Recognition. In *Proceedings of the IEEE Conference on Computer Vision and Pattern Recognition*, pages 770–778, 2016.
- [23] Olivier J Hénaff, Ali Razavi, Carl Doersch, SM Eslami, and Aaron van den Oord. Data-Efficient Image Recognition with Contrastive Predictive Coding. *arXiv Preprint arXiv:1905.09272*, 2019.

- [24] Martin Heusel, Hubert Ramsauer, Thomas Unterthiner, Bernhard Nessler, and Sepp Hochreiter. Gans Trained by a Two Time-Scale Update Rule Converge to a Local Nash Equilibrium. In *Advances in Neural Information Processing Systems*, pages 6626–6637, 2017.
- [25] R Devon Hjelm, Alex Fedorov, Samuel Lavoie-Marchildon, Karan Grewal, Phil Bachman, Adam Trischler, and Yoshua Bengio. Learning Deep Representations by Mutual Information Estimation and Maximization. *arXiv Preprint arXiv:1808.06670*, 2018.
- [26] Ronald Kemker, Marc McClure, Angelina Abitino, Tyler L Hayes, and Christopher Kanan. Measuring Catastrophic Forgetting in Neural Networks. In *Thirty-Second AAAI Conference on Artificial Intelligence*, 2018.
- [27] Youngjin Kim, Minjung Kim, and Gunhee Kim. Memorization Precedes Generation: Learning Unsupervised Gans with Memory Networks. *arXiv Preprint arXiv:1803.01500*, 2018.
- [28] Diederik P Kingma and Jimmy Ba. Adam: A Method for Stochastic Optimization. *arXiv Preprint arXiv:1412.6980*, 2014.
- [29] James Kirkpatrick, Razvan Pascanu, Neil Rabinowitz, Joel Veness, Guillaume Desjardins, Andrei A Rusu, Kieran Milan, John Quan, Tiago Ramalho, Agnieszka Grabska-Barwinska, et al. Overcoming Catastrophic Forgetting in Neural Networks. *Proceedings of the National Academy of Sciences*, 114(13):3521–3526, 2017.
- [30] Lingpeng Kong, Cyprien de Masson d’Autume, Wang Ling, Lei Yu, Zihang Dai, and Dani Yogatama. A Mutual Information Maximization Perspective of Language Representation Learning. *arXiv Preprint arXiv:1910.08350*, 2019.
- [31] Alex Krizhevsky, Geoffrey Hinton, et al. Learning Multiple Layers of Features from Tiny Images. Technical report, Citeseer, 2009.
- [32] Tuomas Kynkäänniemi, Tero Karras, Samuli Laine, Jaakko Lehtinen, and Timo Aila. Improved Precision and Recall Metric for Assessing Generative Models. In *Advances in Neural Information Processing Systems*, pages 3929–3938, 2019.
- [33] Yann LeCun. The MNIST Database of Handwritten Digits. [Http://yann. Lecun. Com/Exdb/Mnist/](http://yann.lecun.com/exdb/mnist/), 1998.
- [34] Ralph Linsker. Self-Organization in a Perceptual Network. *Computer*, 21(3):105–117, 1988.
- [35] Ziwei Liu, Ping Luo, Xiaogang Wang, and Xiaoou Tang. Deep Learning Face Attributes in the Wild. In *Proceedings of International Conference on Computer Vision (ICCV)*, December 2015.
- [36] Sindy Löwe, Peter O’Connor, and Bastiaan S Veeling. Greedy InfoMax for Biologically Plausible Self-Supervised Representation Learning. *arXiv Preprint arXiv:1905.11786*, 2019.
- [37] Qi Mao, Hsin-Ying Lee, Hung-Yu Tseng, Siwei Ma, and Ming-Hsuan Yang. Mode Seeking Generative Adversarial Networks for Diverse Image Synthesis. In *Proceedings of the IEEE Conference on Computer Vision and Pattern Recognition*, pages 1429–1437, 2019.
- [38] Xudong Mao, Qing Li, Haoran Xie, Raymond Y.K. Lau, Zhen Wang, and Stephen Paul Smolley. Least Squares Generative Adversarial Networks. In *The IEEE International Conference on Computer Vision (ICCV)*, Oct 2017.
- [39] Michael McCloskey and Neal J Cohen. Catastrophic Interference in Connectionist Networks: The Sequential Learning Problem. In *Psychology of Learning and Motivation*, volume 24, pages 109–165. Elsevier, 1989.
- [40] Luke Metz, Ben Poole, David Pfau, and Jascha Sohl-Dickstein. Unrolled Generative Adversarial Networks. *arXiv Preprint arXiv:1611.02163*, 2016.
- [41] Takeru Miyato, Toshiki Kataoka, Masanori Koyama, and Yuichi Yoshida. Spectral Normalization for Generative Adversarial Networks. *arXiv Preprint arXiv:1802.05957*, 2018.
- [42] Takeru Miyato and Masanori Koyama. cGANs with Projection Discriminator. *arXiv Preprint arXiv:1802.05637*, 2018.
- [43] Sebastian Nowozin, Botond Cseke, and Ryota Tomioka. f-GAN: Training Generative Neural Samplers using Variational Divergence Minimization. In *Advances in Neural Information Processing Systems*, pages 271–279, 2016.
- [44] Augustus Odena. Open Questions About Generative Adversarial Networks. *Distill*, 2019. <https://distill.pub/2019/gan-open-problems>.

- [45] Augustus Odena, Christopher Olah, and Jonathon Shlens. Conditional Image Synthesis with Auxiliary Classifier Gans. In *Proceedings of the 34th International Conference on Machine Learning-Volume 70*, pages 2642–2651. JMLR. org, 2017.
- [46] Aaron van den Oord, Yazhe Li, and Oriol Vinyals. Representation Learning with Contrastive Predictive Coding. *arXiv Preprint arXiv:1807.03748*, 2018.
- [47] Liam Paninski. Estimation of Entropy and Mutual Information. *Neural Computation*, 15(6):1191–1253, 2003.
- [48] Xue Bin Peng, Angjoo Kanazawa, Sam Toyer, Pieter Abbeel, and Sergey Levine. Variational Discriminator Bottleneck: Improving Imitation Learning, Inverse RL, and Gans by Constraining Information Flow. *arXiv Preprint arXiv:1810.00821*, 2018.
- [49] Ben Poole, Sherjil Ozair, Aäron van den Oord, Alexander A Alemi, and George Tucker. On Variational Lower Bounds of Mutual Information. In *NeurIPS Workshop on Bayesian Deep Learning*, 2018.
- [50] Alec Radford, Luke Metz, and Soumith Chintala. Unsupervised Representation Learning with Deep Convolutional Generative Adversarial Networks. *arXiv Preprint arXiv:1511.06434*, 2015.
- [51] Mehdi SM Sajjadi, Olivier Bachem, Mario Lucic, Olivier Bousquet, and Sylvain Gelly. Assessing Generative Models via Precision and Recall. In *Advances in Neural Information Processing Systems*, pages 5228–5237, 2018.
- [52] Tim Salimans, Ian Goodfellow, Wojciech Zaremba, Vicki Cheung, Alec Radford, and Xi Chen. Improved Techniques for Training Gans. In *Advances in Neural Information Processing Systems*, pages 2234–2242, 2016.
- [53] Akash Srivastava, Lazar Valkov, Chris Russell, Michael U Gutmann, and Charles Sutton. Veegan: Reducing Mode Collapse in Gans Using Implicit Variational Learning. In *Advances in Neural Information Processing Systems*, pages 3308–3318, 2017.
- [54] Christian Szegedy, Vincent Vanhoucke, Sergey Ioffe, Jon Shlens, and Zbigniew Wojna. Rethinking the Inception Architecture for Computer Vision. In *Proceedings of the IEEE Conference on Computer Vision and Pattern Recognition*, pages 2818–2826, 2016.
- [55] Yonglong Tian, Dilip Krishnan, and Phillip Isola. Contrastive Multiview Coding. *arXiv Preprint arXiv:1906.05849*, 2019.
- [56] Naftali Tishby, Fernando C Pereira, and William Bialek. The Information Bottleneck Method. *arXiv Preprint Physics/0004057*, 2000.
- [57] Ngoc-Trung Tran, Tuan-Anh Bui, and Ngai-Man Cheung. Dist-Gan: An Improved GAN Using Distance Constraints. In *The European Conference on Computer Vision (ECCV)*, September 2018.
- [58] Ngoc-Trung Tran, Tuan-Anh Bui, and Ngai-Man Cheung. Improving GAN with Neighbors Embedding and Gradient Matching. In *Proceedings of the AAAI Conference on Artificial Intelligence*, volume 33, pages 5191–5198, 2019.
- [59] Ngoc-Trung Tran, Viet-Hung Tran, Bao-Ngoc Nguyen, Linxiao Yang, et al. Self-Supervised GAN: Analysis and Improvement with Multi-Class Minimax Game. In *Advances in Neural Information Processing Systems*, pages 13232–13243, 2019.
- [60] Ngoc-Trung Tran, Viet-Hung Tran, Ngoc-Bao Nguyen, and Ngai-Man Cheung. An Improved Self-supervised GAN via Adversarial Training. *arXiv preprint arXiv:1905.05469*, 2019.
- [61] Michael Tschannen, Josip Djolonga, Paul K Rubenstein, Sylvain Gelly, and Mario Lucic. On Mutual Information Maximization for Representation Learning. *arXiv Preprint arXiv:1907.13625*, 2019.
- [62] David Warde-Farley and Yoshua Bengio. Improving Generative Adversarial Networks with Denoising Feature Matching. 2016.
- [63] Han Zhang, Ian Goodfellow, Dimitris Metaxas, and Augustus Odena. Self-Attention Generative Adversarial Networks. In *International Conference on Machine Learning*, pages 7354–7363, 2019.

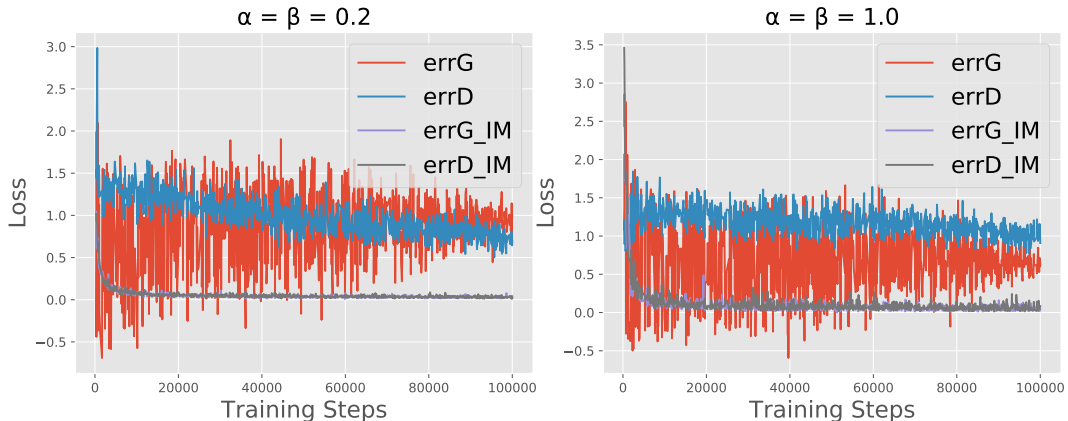


Figure 7: We show that the InfoMax objective loss decays very quickly regardless of the choice of scale for both  $\alpha$  and  $\beta$ .  $\text{errD}$  and  $\text{errG}$  represents the GAN losses for the discriminator and generator respectively, and similarly,  $\text{errD\_IM}$  and  $\text{errG\_IM}$  represents the InfoMax objective losses for the discriminator and generator respectively.

## A Supplementary Results

In this section, we detail supplementary results from various experiments done in the paper.

### A.1 Relative Scale of InfoMax Objective Loss

From Figure 7, we see in both our chosen hyperparameters of  $\alpha = \beta = 0.2$  and the other extreme of  $\alpha = \beta = 1.0$ , the InfoMax objective loss decays very quickly relative to the GAN loss. In practice, we found that  $\alpha = \beta = 0.2$  performs better, which could be attributed to the relative magnitude of the InfoMax objective loss at the start of the training. When  $\alpha = \beta = 0.2$ , the scales of the GAN and InfoMax objective losses are approximately equal initially. We highlight this is the same loss scaling principle applied in [12].

### A.2 Generated Image Samples

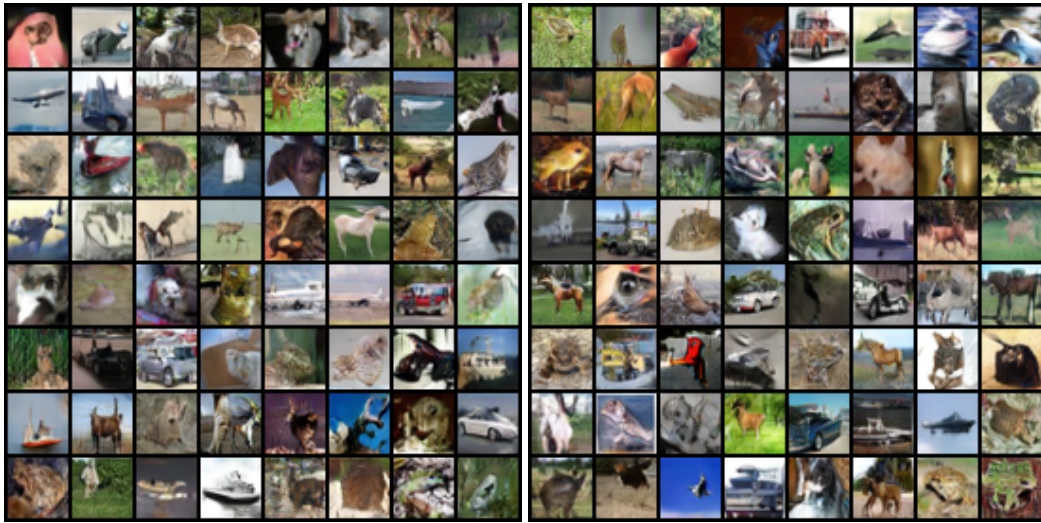
For a qualitative comparison, we present randomly sampled, non-cherry picked images generated by SNGAN and InfoMax-GAN for all datasets in Figures 8 and 10. We qualitatively observe that the images are more diverse and have sharper shapes after the use of an InfoMax objective.

## B InfoGAN Comparison

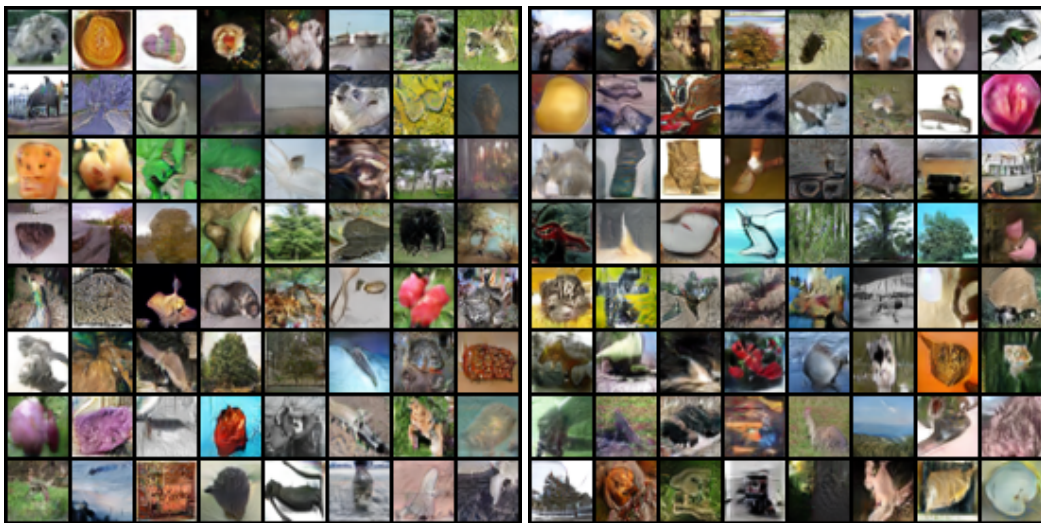
Work	Target Outcome	MI Objective	MI Approximation Technique
InfoGAN [12]	Disentangled representation learning by using an input encoding $c$ to the generator to control its output.	$\mathcal{I}(c; G(z, c))$	Variational Information Maximization [4]
InfoMax-GAN (ours)	Improve image synthesis by reducing catastrophic forgetting of discriminator and mode collapse of generator.	$\mathcal{I}(C_\psi(X); E_\psi(X))$	InfoNCE [46] Task

Table 6: Comprehensive differences with InfoGAN. Our work mainly differs in the intended outcome, the objective to meet the outcome, and the approximation technique needed to solve the objective.

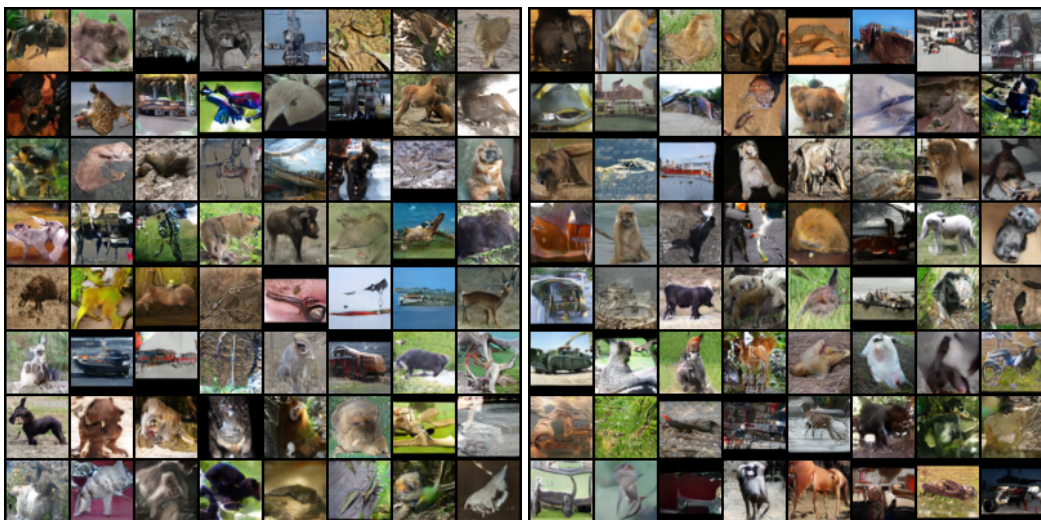
Figure 8: Randomly sampled and non-cherry picked images for SNGAN (left) and InfoMax-GAN (right) for CIFAR-10, CIFAR-100, and STL-10.



(a) CIFAR-10.



(b) CIFAR-100.



(c) STL-10.

Figure 9: Randomly sampled and non-cherry picked generated CelebA images for SNGAN (top) and InfoMax-GAN (bottom).

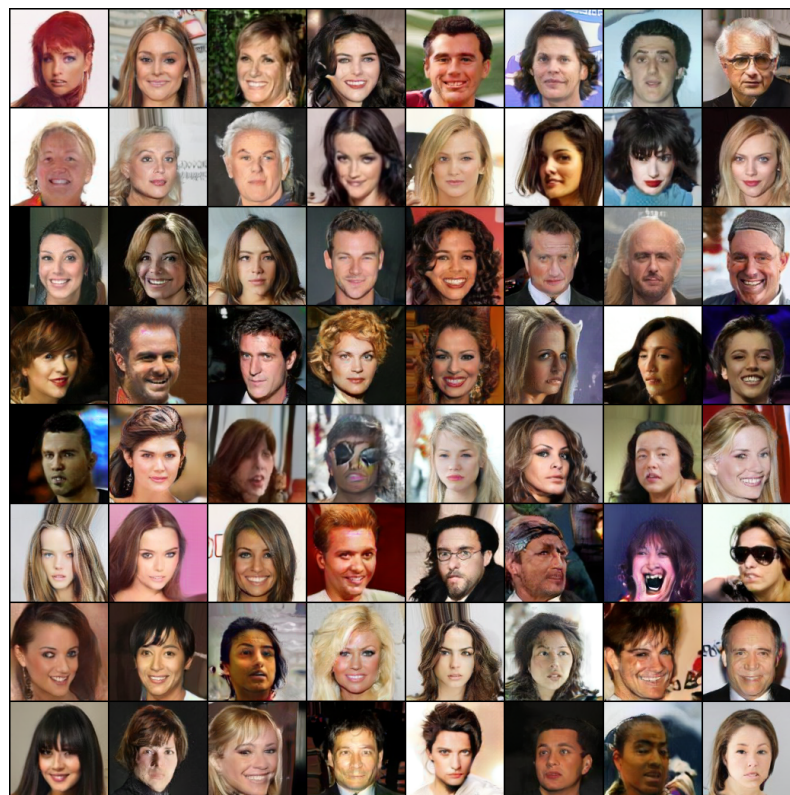
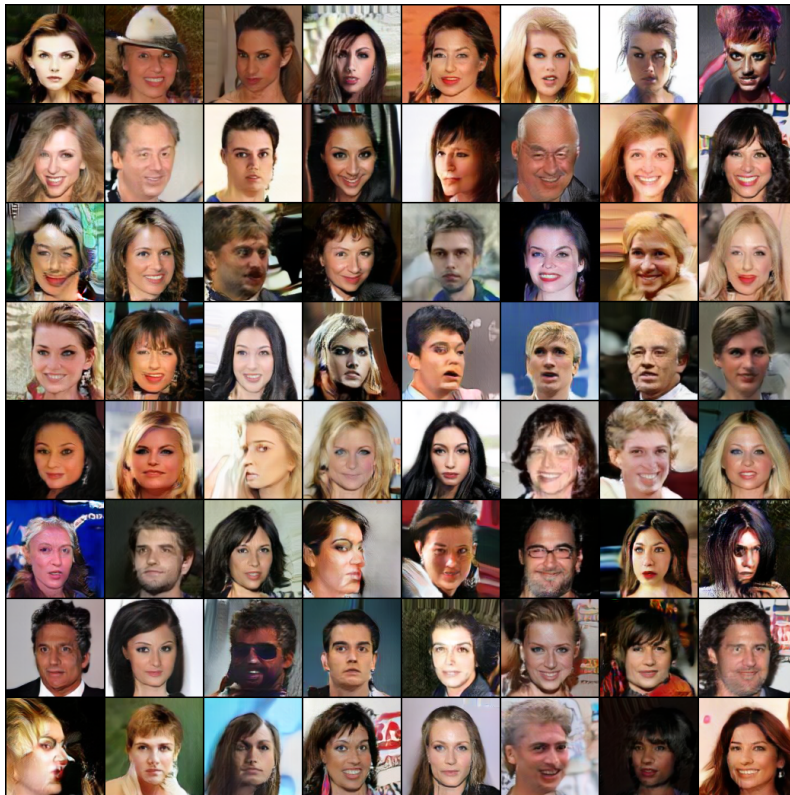
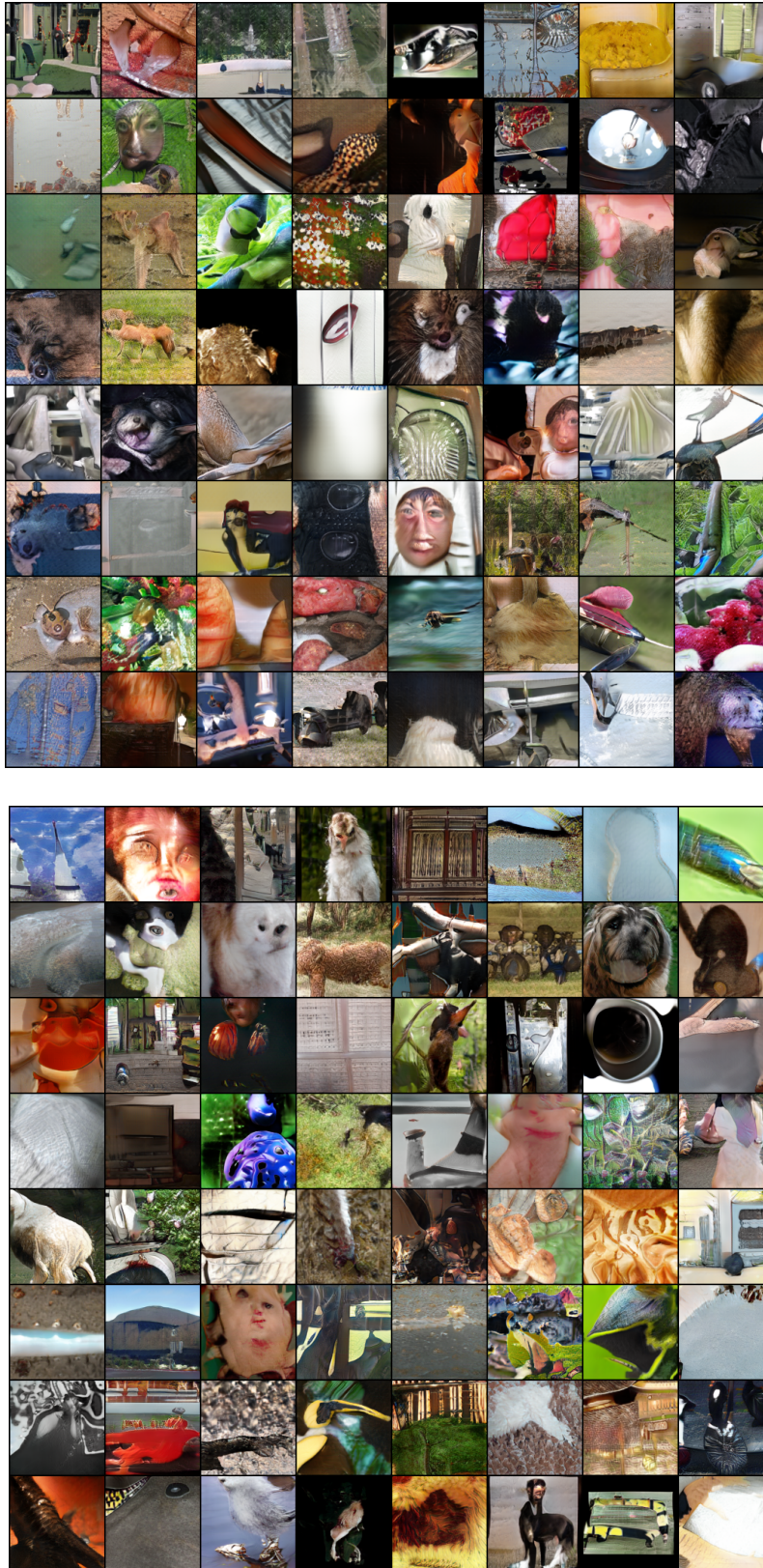


Figure 10: Randomly sampled and non-cherry picked generated ImageNet images for SNGAN (top) and InfoMax-GAN (bottom).



## C Model Architectures

We detail the exact GAN architectures used for all datasets in Tables 7, 8, 9. We also detail the architectures for projecting the local and global features to a higher dimensional RKHS for solving the InfoNCE task in Table 10.

Table 7: Network architectures for the CIFAR-10 and CIFAR-100 datasets, which follows exact settings in [41].

(a) Generator	(b) Discriminator
$z \in \mathbb{R}^{128} \sim \mathcal{N}(0, 1)$	RGB image $x \in \mathbb{R}^{32 \times 32 \times 3}$
Linear, $4 \times 4 \times 256$	ResBlock down 128
ResBlock up 256	ResBlock down 128
ResBlock up 256	ResBlock 128 $\rightarrow$ Local Features
ResBlock up 256	ResBlock 128
BN; ReLU; $3 \times 3$ conv, 3; Tanh	ReLU
	Global Sum Pooling $\rightarrow$ Global Features
	Linear $\rightarrow 1$
(c) Self-supervised Discriminator	
RGB image $x \in \mathbb{R}^{32 \times 32 \times 3}$	
ResBlock down 128	
ResBlock down 128	
ResBlock 128 $\rightarrow$ Local Features	
ResBlock 128	
ReLU	
Global Sum Pooling $\rightarrow$ Global Features	
Linear $\rightarrow 1$ ; Linear $\rightarrow 4$	

Table 8: Network architectures for the STL-10 dataset, which follows exact settings in [41].

(a) Generator	(b) Discriminator
$z \in \mathbb{R}^{128} \sim \mathcal{N}(0, 1)$	RGB image $x \in \mathbb{R}^{48 \times 48 \times 3}$
Linear, $6 \times 6 \times 512$	ResBlock down 64
ResBlock up 256	ResBlock down 128
ResBlock up 128	ResBlock down 256
ResBlock up 64	ResBlock down 512 $\rightarrow$ Local Features
BN; ReLU; $3 \times 3$ conv, 3; Tanh	ResBlock 1024
	ReLU
	Global Sum Pooling $\rightarrow$ Global Features
	Linear $\rightarrow$ 1
(c) Self-supervised Discriminator	
RGB image $x \in \mathbb{R}^{48 \times 48 \times 3}$	
ResBlock down 64	
ResBlock down 128	
ResBlock down 256	
ResBlock down 512 $\rightarrow$ Local Features	
ResBlock 1024	
ReLU	
Global Sum Pooling $\rightarrow$ Global Features	
Linear $\rightarrow$ 1; Linear $\rightarrow$ 4	

Table 9: Network architectures for the CelebA and ImageNet datasets. This follows the exact settings in the official SNGAN code [1].

(a) Generator	(b) Discriminator
$z \in \mathbb{R}^{128} \sim \mathcal{N}(0, 1)$	RGB image $x \in \mathbb{R}^{128 \times 128 \times 3}$
Linear, $4 \times 4 \times 1024$	ResBlock down 64
ResBlock up 1024	ResBlock down 128
ResBlock up 512	ResBlock down 256
ResBlock up 256	ResBlock down 512 $\rightarrow$ Local Features
ResBlock up 128	ResBlock down 1024
ResBlock up 64	ResBlock 1024
BN; ReLU; $3 \times 3$ conv, 3; Tanh	ReLU
	Global Sum Pooling $\rightarrow$ Global Features
	Linear $\rightarrow$ 1
(c) Self-supervised Discriminator	
RGB image $x \in \mathbb{R}^{128 \times 128 \times 3}$	
ResBlock down 64	
ResBlock down 128	
ResBlock down 256	
ResBlock down 512 $\rightarrow$ Local Features	
ResBlock down 1024	
ResBlock 1024	
ReLU	
Global Sum Pooling $\rightarrow$ Global Features	
Linear $\rightarrow$ 1; Linear $\rightarrow$ 4	

Table 10: InfoNCE projection architectures, which follow what were proposed in [25]. In practice, we extract the local features and global features from the penultimate and final residual blocks of the discriminator respectively. This decides the corresponding values of feature depth  $K$ .

(a) Local features projection architecture.	(b) Global features projection architecture.
$1 \times 1$ Conv, $K$ ; $1 \times 1$ Conv, $R \rightarrow$ Shortcut	Linear $\rightarrow K$ ; Linear $\rightarrow R \rightarrow$ Shortcut
ReLU	ReLU
$1 \times 1$ Conv, $R +$ Shortcut	$1 \times 1$ Conv, $R +$ Shortcut